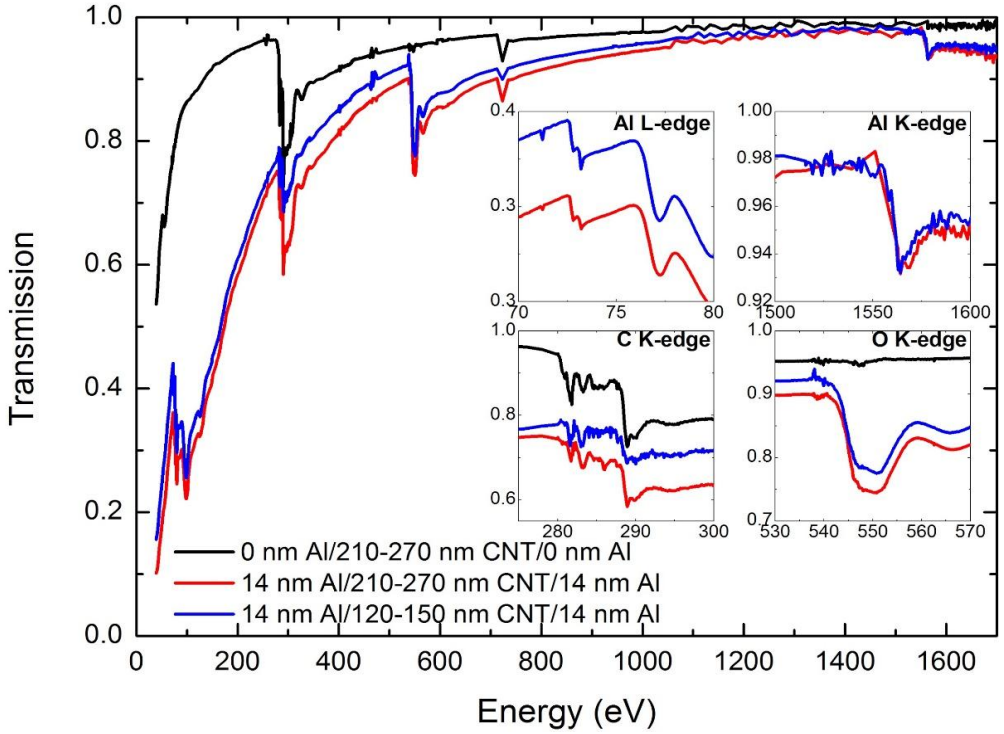

Fig. 16 - Comparison between the transmission curves of three CNT samples.

The samples with an aluminum coating on the CNT membrane would show important surface oxidation, clearly visible in the very structured Al L-edge (see the presence of a double edge between 72 eV and 75 eV in the inset of the Al L-edge of Fig. 16).

In the region around 700 eV there is a signal ascribable to Fe L-edge. Unfortunately, the step energy used in that spectral region is not sufficient to reveal a clear signal. We have increased the number of points in that region in the x-ray transmission measurement of the next experimental campaign performed at BESSY II in July 2020 (see x-ray mapping in the following section).

These experimental data were analyzed according to the transmission model described in the previous paragraph, by using the material each layer is made of. In particular, we considered layers of Al, Al_2O_3, C and Fe. The membrane, indeed, is mainly composed of carbon atoms with a residual percentage of Fe atoms, used as precursors in the CNT growing process.

The layer thickness of each material together with 3σ statistical uncertainty arising from best fit are reported in Table 13.

The best fit results in Figures 17-19 show the presence of a significant amount of aluminum oxide. Though the significant oxidation of aluminum is a reliable evidence, also confirmed by XPS measurements, the derived quantity may be overestimated by the presence of some water on the surface, not taken into account in the model, which adding oxygen forces the fit to overestimate the amount of aluminum oxide.

Table 13: Layer thickness of each material (Al, Al_2O_3, C and Fe) with 3σ statistical uncertainty and nominal thickness for all filters.

	Best fit thickness (nm) or areal density (10^{-7} g/cm^2)				Nominal thicknesses (nm)	
Filters	**Al**	**Al_2O_3**	**C areal density**	**Fe**	**Al**	**CNT**
LAOF-CNT2-C1B3-F18 (68)	-	-	36.0 (0.7)	1.4 (0.1)	-	210-270
LAOF-CNT2-C1B3-F19 (69)	1.8 (1.2)	31.7 (1.4)	41.7 (1.4)	0 (0.7)	14 x 2	210-270
LAOF-CNT2-C1B2-F02 (52)	1.8 (0.7)	28.2 (1.1)	25.6 (0.9)	0 (0.5)	14 x 2	120-150

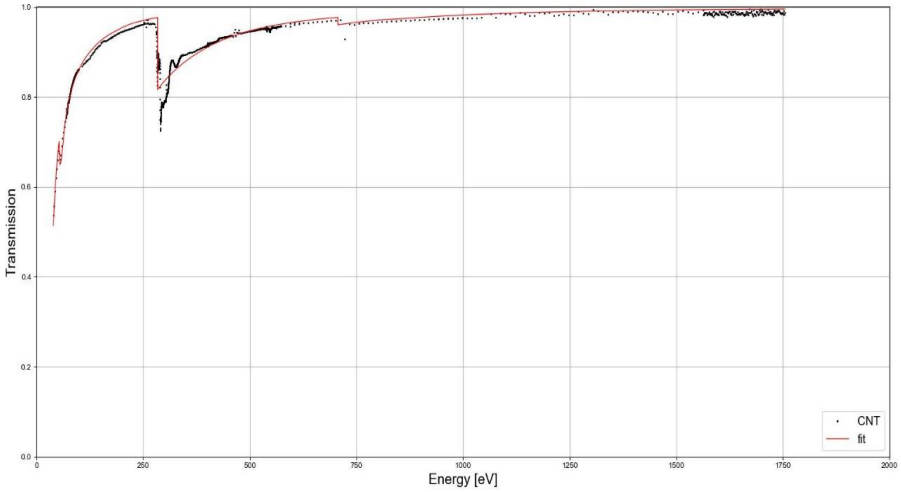

Fig. 17 - Experimental data (black points) of measured LAOF-CNT2-C1B3-F18 0 nm Al/ 210-270 nm CNT/ 0 nm Al filter and the best fit on materials (red line).

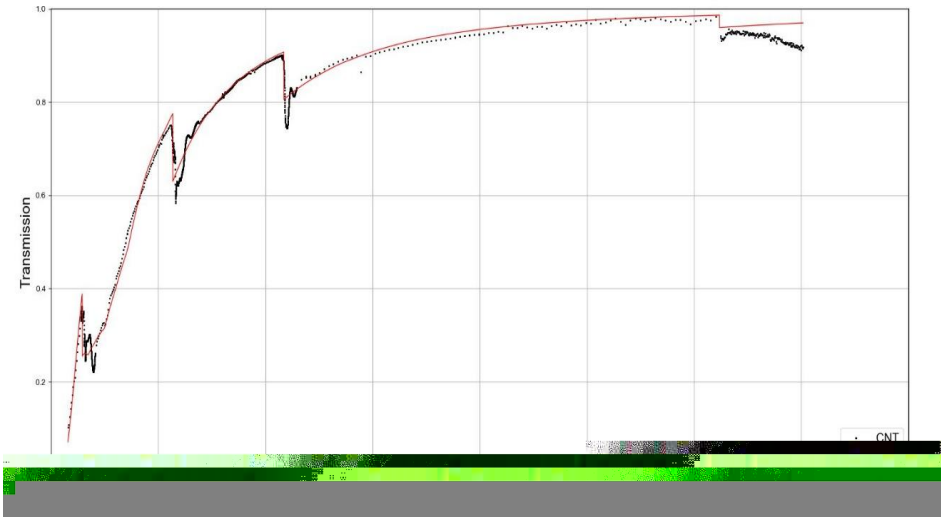

Fig. 18 - Experimental data (black points) of measured LAOF-CNT2-C1B3-F19 14 nm Al/ 210-270 nm CNT/ 14 nm Al filter and the best fit on materials (red line).

Fig. 19 - Experimental data (black points) of measured LAOF-CNT2-C1B2-F02 14 nm Al/ 120-150 nm CNT/ 14 nm Al filter and the best fit on materials (red line).

Data on the PI/Al + PI mesh sample filters were also analyzed according to the transmission model, by using the following materials: Al, Al_2O_3, PI, plus two mesh parameters, thickness and open area (OA). The scattering factors f2 used in modeling each element edge were retrieved from Luxel samples in previous campaigns. Indeed, one of the main results is that edges are not much different from those seen in Luxel samples, pointing towards very similar materials and manufacturing/deposition techniques both for the aluminum coating and the polyimide membrane. Each layer thickness and their 3σ statistical uncertainties from the best fit are reported in Table 14.

Table 14: Layer thickness of each material (Al, Al_2O_3, PI, PI mesh thickness and OA) with 3σ statistical uncertainty and nominal thickness for all filters.

	Best fit thicknesses					Nominal thicknesses			
Filters	Al (nm)	Al_2O_3 (nm)	PI (nm)	PI mesh (μm)	OA (%)	Al (nm)	PI (nm)	PI mesh (um)	OA (%)
OIT-TF111-80	23.0 (0.9)	11.4 (0.8)	36 (3)	5 (2)	97.8 (0.2)	15 x 2	55	18	97
OIT-TF111-81	19.6 (0.8)	10.9 (0.7)	49 (3)	49 (50)	93.6 (0.2)	15 x 2	55	18	97

The best fit in Figures 20-21 follows the data well enough below about 900 eV, however a different slope of the data can be clearly seen in both datasets at the higher end of the energy range. This effect is mainly due to two issues: 1) the position of the beam spot changes with the monochromator angle (the effect increasing with E), thus hitting different spots of the mesh, this effect results in an "effective" open area, as sampled by the beam spot, which varies with the energy when the mesh pitch is comparable with the spot size; 2) above 1400 eV, there is an experimental problem with the beamline, where diffused light enters spuriously in the monochromator, making the Al K edge measurement unreliable.

Notwithstanding, the best fit parameters for Al and Al oxide are in good agreement with the nominal and expected values (about 14 nm), whereas the PI membrane is slightly underestimated because the fit encounters some difficulty in separating the membrane contribution from the mesh one (being of the same material). The same problem arises in estimating the PI mesh thickness. The OA is actually the effective value sampled by the beam spot.

Overall, these samples show an X-ray transmission and material characteristics very similar to Luxel filter samples, except for the effect of the mesh. It would be interesting to further investigate meshless samples and to check the PI mesh quality with a microscope, in order to verify the nominal parameters and the absence of inhomogeneities due to mesh growth on the PI substrate. It would also be useful to attempt out of focus measurements in a synchrotron beamline, to average out the effect of the mesh on the transmission curve.

Fig. 20 - Experimental data (black points) of measured OIT-TF111-80 15 nm Al/ 55 nm PI/ 15 nm Al + PI mesh filter and the best fit on materials (red line).

Fig. 21 - Experimental data (black points) of measured OIT-TF111-81 15 nm Al/ 55 nm PI/ 15 nm Al + PI mesh filter and the best fit on materials (red line).

Measurements on a 140 nm polyimide film, without coating to investigate the polymer, manufactured by OXFORD has been performed at BEAR on beam scientist time on October 12-15, 2020. Results are being analyzed and will hopefully be reported before the Final Review.

;"J $%&()$ 7 (3381K$(-$-+.$FL6&%6M<$C.(7/81.$

In order to perform an investigation on the spatial uniformity of the manufactured large area filter samples, we have performed a full illumination x-ray transmissivity map at the XACT-facility of the INAF – Osservatorio Astronomico di Palermo – Italy. In particular, we have used the 35 meter long vacuum beam line, an electron impact multi-anode x-ray source (0.1-20 keV) and a MicroChannel Plate (MCP) detector with a circular sensing surface of 40 mm diameter (Fig. 22).

Fig. 22 – Schematic layout of the experimental set-up used at the XACT facility of INAF-OAPA to perform x-ray full illumination transmission mapping of few filter samples.

The investigated filter samples are an OXFORD aluminized polyimide film supported by a polyimide mesh and an AMETEK aluminized carbon nano tube (CNT) self-standing film. The main characteristics of the two filters, along with the mesh parameters, are summarized in table 15.

Table 15: Main characteristics of the two filters measured at the XCAT fCILITY beamline AT INAF-OAP to derive an x-ray mapping.

Filter	Filter Area (mm^2)	Al (nm)	Film (nm)	mesh (μm)	Mesh features (μm)	OA (%)
W3a-#03	square 82 x 82	2 x 15-20	Polyimide 140	Polyimide 18	PI hexagonal pattern bar width 20, pitch 762	95
LAOF-CNT1-C1B1-F05	square 82 x 82	2 x 11	CNT 120-150		No mesh	100

To cover the entire surface of a filter with the smaller size MCP detector, the filter was mounted on an x-y micro-motion system and several images have been taken to form a mosaic covering the entire useful surface. Notice that only the inner 34 mm diameter area of the MCP has been used to avoid edge effects of the detector sensitivity. Fig. 23 shows the MCP position over the useful surface of the filter and highlights that a 4x4 matrix of circular images of MCP is required to cover the entire filter.

Fig. 23 – Filter mapping of the full 82 mm x 82 mm square filter area by a mosaic of 16 circular shape MCP images with 34 mm diameter usefull sensitive area.

Each filter was illuminated with a pseudo-monochromatic x-ray beam consisting of characteristic fluorescent lines and bremsstrahlung radiation emitted by the impact of electrons on the target anode in the x-ray source. A thin film (filter) made of the same material as the anode is used along the x-ray path to minimize the contribution of the bremsstrahlung continuum. Used anode and the correspondent lines are indicated in the table 16.

Table 16: Anodes and filters used to generate quasi monochromatic x-ray beam and the corresponding energy of the fluorescent lines.

Anode (line)	Bremsstrahlung Filter	Energy (keV)
C (Kα)	Polypropylene 1 μm	0.28
Cu (L)	Cu 0.1 μm	0.93
Al (Kα)	Al 10 μm	1.49

In order to account for time fluctuations of the x-ray beam intensity a direct beam measurement (OPEN) was taken before and after every measurement with the filter in front of the MCP detector in one of the 16 positions of the mosaic (POS) required to scan the entire filter surface as indicated in Figure 23. OPEN and POS measurements are taken with variable integration time in order to get the same total counts and thus similar statistical uncertainty. Finally, in order to remove the MCP noise, a long exposure background image was taken with the source off. The filter transmission map is then obtained with the following formula:

where %&' refers to the MCP acquisition through the filter, ()* refers to background acquisition, &%+,- and &%+,. refers to the direct beam MCP acquisitions taken before and after the POS acquisition; moreover, the subscript /01 refers to the counts collect per pixel and the subscript 0234 refers to the exposure live time (corrected for the dead time) of each measurement.

60.758$9#*6)+%; :);<; :6=>$

Unfortunately, the filter LAOF-CNT1-C1B1-F05, after being safely mounted inside the test chamber, was found damaged during the x-ray tests. One possibility is that it suffered the flow of air caused by the rough pump in the first phase of the chamber venting process. Fig. 24 (left panel) shows a transmission image of filter LAOF-CNT1-C1B1-F05 taken before realizing that it was broken, while Fig. 24 (right panel) shows the photo taken after having removed it from the test chamber. The x-ray transmissivity image highlights very well the parts where there are remaining pieces of CNT film.

Fig. 24 – Transmission image of the LAOF-CNT1-C1B1-F05 at rebin 4 (left panel). Picture of the same filter after the test chamber unmount (right panel).

60.758$?@A$B=@

Figure 25 shows the images of counts transmitted by the filter W3a-#03 irradiated with Carbon anode at different spatial resolution, starting with full MCP resolution whith 1 pixel = 100 μm x 100 μm, (a) and then rebinning with larger pixels from 2x2 (b) up to 32x32 (f).

Fig. 25 – Images of the counts detected over the full area of the filter W3a -#03 irradiated by a C anode at different pixel binning. (a) full resolution (1 pixel = 100 μm x 100 μm), (b) rebin 2, (c) rebin 4, (d) rebin 8, (e) rebin 16, (f) rebin 32.

In every single image, it's easy to notice the larger number of counts collected in the overlapping regions, this effect is cancelled out by dividing for the exposure time when calculating the transmission map. Given the large number of pixels in the image (~700000 in full resolution) and moderate statistics, due to the low flux rate and limited time exposures, it's not unlikely to have few pixels of the images with zero counts or some pixels for which the count rate of the OPEN or POS measures are lower than the detected background rate. In these cases, the calculation of the formula for transmissivity T would lead to negative or infinite values. For this reason, the x-ray transmission for these pixels has been artificially set to zero if the problem occurred on the numerator and to 9999 if it occurred on the denominator of the transmissivity formula.

Fig 26 shows the distribution of x-ray transmission of W3a-#03 filter at the Carbon Kα energy (0.28 keV) for all pixels of the image taken with a rebin 4. The plot shows a large number of pixels with T close to 0, however, these points are not statistically significant because they are either pixels where trasmissivity was artificially set to zero, as previously explained, or pixels which present a very low transmissivity since they are very close to the frames that partially block the beam. For these reasons, pixels with a T value less than 0.1 were not considered in the calculation of the average transmissivity.

Figure 26 – Distribution of the x-ray transmission of W3a-#03 filter at the Carbon Kα energy (0.28 keV) for all pixels of the image taken with a rebin 4x4.

The transmissivity images and related distributions obtained using the carbon anode are shown respectively in Fig. 27 and Fig. 28. Table 17 shows the mean transmissivity values (Tmean) and associated standard deviation (σ) at different rebins for the three different energies of Carbon, Copper and Aluminum.

Fig. 27 – Transmissivity maps of W3a- # 03 at the C-Kα energy (0.28 keV) at full spatial resolution (a), rebin 2 (b), rebin 4 (c), rebin 8 (d), rebin 16 (e), rebin 32 (f).

As shown in Tab. 17 and Fig. 28, the transmissivity distributions at small rebins are not reliable, partially because of the poor counting statistics, but mainly because the pixels are small with respect to the mesh pitch and thus they sample different portions of the mesh wires introducing an artificial fluctuation of transmission. Fig. 29 shows a single hexagonal polyimide mesh cell compared with rebin pixels 1, 2 and 4. Starting from rebin 4, the average transmissivity value consolidates towards a reliable value.

Table 17: Mean value and standard deviation of the transmissivity distribution measured on W3a-#03 filter with different rebins at the C-Kα (0.28 keV), Cu-L (0.93 keV), and Al-Kα (1.49 keV) energies, respectively.

Rebin	C (277eV)		Cu (930eV)		Al (1490eV)	
	T_{MEAN}	σ	T_{MEAN}	σ	T_{MEAN}	σ
5%	0.6	0.65	0.7	0.8	0.7	0.8
6%	0.5	0.40	0.6	0.5	0.6	0.5
7%	0.72	0.12	0.90	0.15	0.93	0.15
8%	0.72	0.06	0.90	0.08	0.93	0.08
59%	0.72	0.04	0.90	0.05	0.93	0.05
:6 %	0.72	0.04	0.90	0.04	0.93	0.05

Figure 28 – Distribution of the x-ray transmission of W3a-#03 filter at the Carbon Kα energy (0.28 keV) for all pixels of the images taken at different binning: (a) full resolution, (b) rebin 2, (c) rebin 4, (d) rebin 8, (e) rebin 16, (f) rebin 32. The curves are obtained by removing the pixels with T values lower than 0.1.

Fig. 29 – Schematic drawing of an hexagonal cell of the polyimide support mesh compared to rebin pixels 1, 2 and 4. Dimensions are expressed in mm.

Fig 30 shows the transmissivity images (rebin 32) and the relative distributions at the characteristic energies of Cu-L (0.93 keV) and Al-Kα (1.49 keV), respectively.

Figure 30 – (a) Transmissivity image (rebin 32) of W3a-#03 filter at the Cu-L energy (0.93 keV), and (b) relative transmission distribution of all pixels with T > 0.1. (c) Transmissivity image (rebin 32) of W3a-#03 filter at the Al-Kα energy (1.49 keV), and (d) the relative transmission distribution.

In order to evaluate the statistical significance of the width of the transmission distributions, and infer to what extent it can be ascribed to a real filter non uniformity, we have estimated the Poissonian statistical error on transmissivity weighted for the different exposure times of the individual areas marked with different colors in Fig. 31. In particular, we have considered the rebin 16 map at the C-Kα energy (0.28 keV).

Fig. 31 – Exposure map of the filter image mosaic. Light red corresponds to single time coverage, white is four times coverage.

The statistical width of the transmission distribution was obtained by estimating the expected number of counts per pixel in OPEN and POS measurements under the hypothesis of spatially uniform filter and calculating the relative error starting from the above reported equation to calculate transmission. The derived 1σ relative statistical uncertainty is 5.5%. This value is comparable to the measured relative uncertainty reported above in Table 16 (0.043/0.719 = 6%) indicating that the W3a–#03 appears to be spatially uniform within the statistical uncertainty of our measurements.

Finally, it is possible to compare the experimental average transmissivity value of the filter W3a-#3 at the various energies with the theoretical value calculated assuming a polyimide thickness of 140 nm, a total layer of Al of 40 nm and a 95% open area mesh. Table 18 makes a comparison between the two transmissivities for the three available energies. The transmissivity of the filter W3a-# 03 found experimentally is compatible with the theoretical values within the uncertainties.

Table 18: Comparison between measured average transmission and modeled one at the three available energies. Namely: Carbon Kα energy (0.277 keV), Copper L energy (0.93 keV), and Aluminum Kα energy (1.49 keV).

Energy (keV)	! !"#$ "	#"	! %&'"("
0.28	0.72	0.04	0.75
0.93	0.90	0.04	0.88
1.49	0.93	0.05	0.93

;"N$%&()$ 7 (3381K$(-$-+.$*<?&@AB$C.(7/81.$,D$$?@22E$$FF

X-Ray transmission mapping measurements were performed on a large size sample manufactured by OXFORD, made of a polyimide layer coated with a thin Al layer on each side and supported by a polyimide mesh. The sample filter has the same size of a single quadrant of the Athena WFI Large Detector Array Optical Blocking Filter. The imaging aims to evaluate spatial uniformity, by measuring a transmission spectra over the full energy range in each of the 28 position reported in the schematic layout (Fig. 32).

Fig. 32 - Positions of the X-ray measurements performed on filter W3a#06 (Al/PI/Al + PI mesh).

The sample filter nominal layer thicknesses, along with its PI mesh characteristics, are reported in Table 19.

Table 19: Nominal layer thickness for the Al/PI/Al + PI mesh Oxford filter sample measured at BESSY II.

Filter	Al (nm)	Polyimide (nm)	Pi mesh (μm)	OA (%)	Mesh features (μm)
W3a#06	15-20x2	140	17±1l	95	bar Width 20 pitch size 800

The X-ray mapping measurements performed @PTB-EUV beamline on the OXFORD filter sample are in the energy range 50 eV to 1800 eV, using coarser energy steps to obtain the full transmission curve at each position in a reasonable time, as reported in table 20.

Table 20. Energy steps adopted for the x-ray transmission mapping at PTB EUV.

Energy range (eV)	50 – 600 eV	600 - 1800 eV		
Filter	Energy Step (eV)		N of data points at each position$	N of positions$
W3a#06	10	50	79	28

The transmission mapping on the square sample W3a#06 (Al/polyimide with PI mesh), acquired in different filter positions, are reported in Figures 33-35. Data corresponding to the bottom horizontal line (positions 1-7 in Fig. 30) and the central horizontal line (positions 22-28 in Fig. 32) are reported in figs. 33 and 34, respectively.

Fig. 33 - Experimental transmission of W3a#06 filter mapped in seven positions along the horizontal bottom line (left) and along the horizontal central line (right).

From figure 33, the maximum relative difference in transmission between positions belonging to the horizontal bottom line is about 6%, whereas the maximum relative difference in transmission between positions belonging to the horizontal center line (22-28) is about 9%. A plot of the transmission data obtained by mapping along the vertical central line (positions 4, 11, 18, 25) and the vertical right line (positions 7, 8, 21, 22) together with the mapping obtained along a left diagonal

line (positions 28, 16, 12, 4 in Fig. 30) and a right diagonal line (positions 4, 10, 20, 22 in Fig. 30) are displayed in Fig. 34.

Fig. 34 - Experimental transmission of W3a#06 filter mapped in eight positions along the vertical central and right lines (left) and mapped in seven positions along the left and right diagonals (right).

The maximum relative difference in transmission is about 9% between the two vertical lines (positions 4,11,18,25) and (positions 7,8,21,22), whereas it is about 8% between the two diagonals (positions 28,16,12,4) and (positions 4,10,20,22). All of the above differences could in theory either be due to local differences in the PI or Al layer thicknesses or, more likely, to the beam spot hitting different portions of the mesh at each position, thus resulting in a difference in the mesh open area. To further investigate this, a best fit analysis based on filter materials (polyimide, Al, Al_2O_3) along with mesh parameters (thickness and open area) was performed in two positions with strikingly different transmission curves, namely positions 7 and 18 (see Fig. 35).

Fig. 35 - Experimental transmission of W3a#06 filter mapped in positions 7 and 18, along with the best fits on materials.

Both best fits in Fig. 35 look overall good. The parameters obtained from the fit are reported in table 21.

Table 21: Layer thickness of each material (Al, Al_2O_3, polyimide and polyimide mesh) and open area (OA) with 3σ statistical uncertainty and nominal thickness for two positions on filter W3a#06 corresponding to maximum and minimum transmission.

	Best fit thicknesses (nm)					*Nominal thicknesses (nm)*			
Filters	**Al**	**PI**	**Al_2O_3**	**PI mesh (µm)**	**OA (%)**	**Al**	**PI**	**PI mesh (µm)**	**OA (%)**
W3a#06 - Pos 7	18±2	156±4	14±3	14±3	87.1±0.6	2 x15-20	140	18±2	95
W3a#06 - Pos 18	18±2	149±3	13±2	15±9	96.0±0.6	2 x15-20	140	18±2	95

Table 21 shows that the major difference between the transmission curves in positions 7 and 18 is due to a different portion of the mesh being hit by the beam spot (see the changes in the open areas). The total amount of aluminum oxide is in good agreement with the expected value of about 3.5 nm per layer side, whereas the polyimide is slightly overestimated. However, a small difference of about 7 nm is seen in the PI thickness, just within the errors associated with the fits. Thus, in a filter with a PI mesh with mesh cell pitch as small or smaller than the beam spot size, we cannot detect significant differences in either the PI or the Al layer. Presumably, the filter looks homogeneous enough for what concerns the membrane. More insight could be gained by measuring a filter without the mesh, or by performing measurements in an "out of focus" setup, where the beam spot can hit several mesh cells at once, thus averaging out the differences at different positions due to different portions of a single mesh cell being hit.

The X-ray beamline PTB EUV of the Physikalisch Technische Bundesanstalt at BESSY II in Berlin – Germany was used to perform X-ray transmission measurements in the energy range 225 eV - 1800 eV on a different type of filter material, a carbon nanotubes mesh (CNT), which has been investigated in the last part of the LAOF project and will be further investigated in LAOF-CCN. Data near the C K-edge were not acquired by the beam scientists due to contamination of the chamber. The sample measured was the AMETEK filter **LAOF-CNT1-C1B1-F01** CNT without Al, mounted on a square frame which is the baseline of one single quadrant of the Athena WFI Large Detector Array (LDA) Optical Blocking Filter (OBF). The sample filter nominal layer values are reported in table 22.

Table 22: Nominal layer thicknesses for the CNT Ametek filter sample measured at BESSY II.

Filter	**Al (nm)**	**CNT (nm)**	**Density**
LAOF-CNT1-C1B1-F01	-	120-150	LOW

The main goals of the test campaign were:

$

1)$To perform an X-ray mapping to assess spatial uniformity of a large size CNT sample;

2)$To derive the CNT layer thickness;

3)$To derive the amount of Fe present in the CNT membrane.

A schematic representation of the CNT square sample filter is reported in fig. 36, along with the positions for the X-ray mapping (1 to 16 in red).

Fig. 36 – Square CNT without Al coating and mapping positions

The energy steps used are reported in table 23. The reason for the small step at low energy is to better acquire and then model each material thickness, also decreasing the associated error in layer thickness.

Table 23:. Energy steps adopted in different energy ranges.

Holder 2	225 - 730 eV	730-1800 eV	N data per position	N positions	N data points
6=IDJH$	KLH>MN$6BGHB$Q		$	$	$
LAOF-CNT1-C1B1-F01	2	10	357	16	5712

Data obtained at the different 16 positions are plotted in Fig 37 all together, to show the CNT membrane uniformity. A first important result is that the filter is very transparent, with T ranging between 0.925 and 1. A second result is that, as can be seen in Fig 37, the CNT mesh is quite uniform, with the largest difference in transmission between position 16 (bottom curve) and 8 (upper curve), only noticeable in the C K post-edge (320 eV - 380 eV). In any case, since the filter is very

transparent, the difference in transmission does not exceed about 0.007, so that the **Δ**T/T remains below 1%.

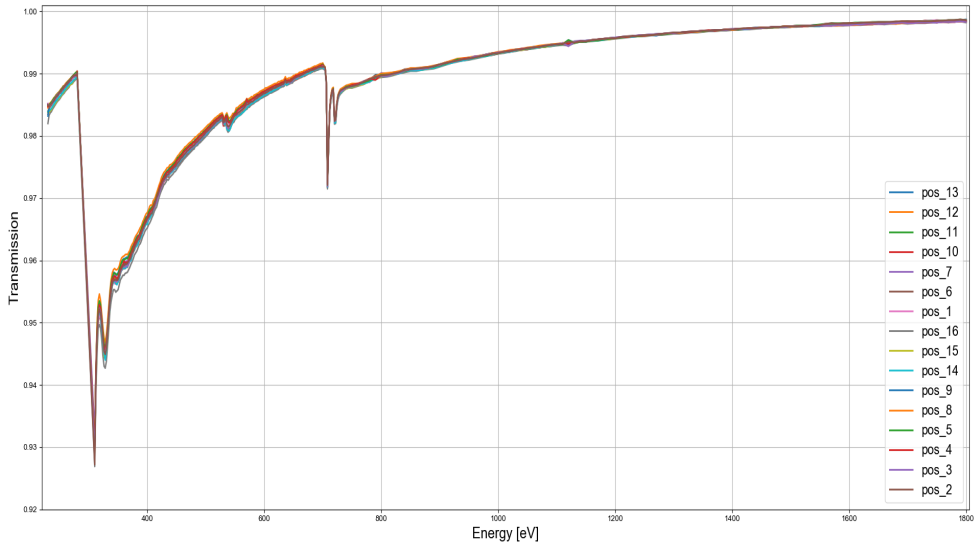

Fig.37 – Transmission curve of CNT sample LAOF-CNT1-C1B1-F01 measured in 16 different positions.

A fit according to the developed model of transmission, using Henke tabulated values of the scattering factors, was then performed over the 16 curves including the elements: C, O and Fe. Data and fit for position 13 are plotted in fig 38 as an example. The results obtained for the areal densities of each element are reported in table 24.

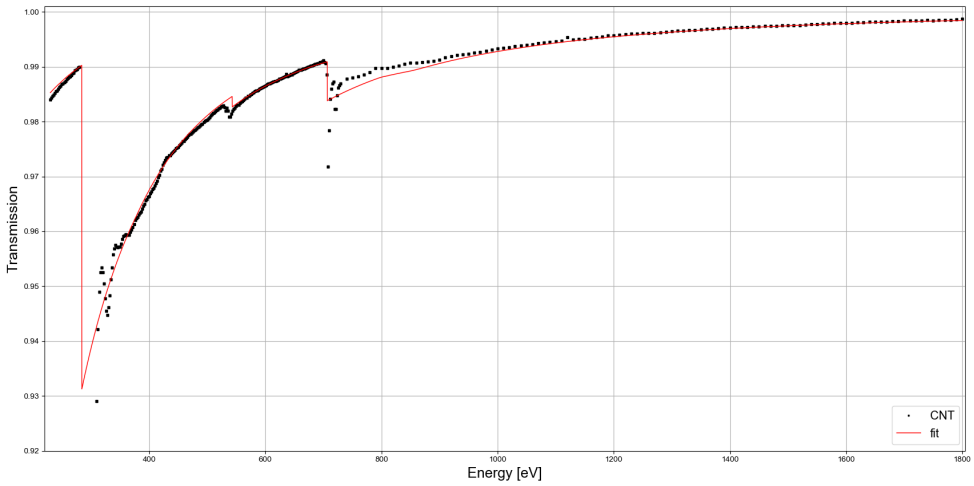

Fig. 38 – Transmission of CNT sample LAOF-CNT1-C1B1-F01 at centre position 13 (black dots) and fit (red line).

Table 24: areal densities for each element and error in parenthesis. The bottom curve (position 16) is highlighted in green, the upper one (position 8) is highlighted in red.

$	***Areal densities (10^{-7} g/cm^2)*** $		
Positions	**C**	**O**	**Fe**
#1$	#-";$O!"-Q$	!"2$O!"/($	/"+$O!"/($
#0$	#-"/$O!"-Q$	!"+$O!"($	/"2$O!"/($
#/ $	#-"0$O!"-($	!";$O!"/Q$	/"2$O!"/($
#($	#-"($O!"-Q$	#"!$O!"/($	/"0$O!"/($
#- $	#-"0$O!"-($	!";$O!"/Q$	/"0$O!"/($
##$	#-"/$O!"-Q$	#"!$O!"/($	/"0$O!"/($
#! $	#-"0$O!"-($	!";$O!"/Q$	/"/$O!"/Q$
2$	#-"-$O!"-Q$	!";$O!"(Q$	/"0$O!"/($
+$	##";$O!"-($	!"1$O!"(($	/"0$O!"/($
; $	#-"#$O!"-($	!"2$O!"/($	/"0$O!"/($
1$	#-"1$O!"-($	!"+$O!"($	/"/$O!"/Q$
0$	#-"#$O!"-($	!"2$O!"($	/"0$O!"/($
/ $	#-"-$O!"-Q$	!"1$O!"($	/"1$O!"/($
#$	#-"0$O!"-($	!"1$O!"($	/"0$O!"/($
- $	#-"0$O!"-($	!"2$O!"/($	/"0$O!"/($
($	#-"0$O!"-($	!"2$O!"($	/"0$O!"/($

As it can be seen from table 24, the CNT mesh is slightly thinner in positions 8,9,5,4,7,13 (the center-right side internal part of the filter), and slightly thicker in positions 16, 6, 14 (left border), 10,12 (right border) and 1,2,3 (bottom border). The oxygen amount is rather uniform, within the error, and it is probably due to water or OH groups attached to the CNT mesh. The amount of iron is also very uniform, as it is used as a catalyst in the reaction to obtain CNT (thus it should depend on the amount of C).

In table 25 we report the ratio between each element areal density (the best fit parameter), divided by its atomic mass. By comparing these two numbers for C and Fe one can infer the ratio between atoms of each element, which is between 12:1 and 13:1.

Table 25: areal density of the number of atoms for C and Fe.

Position	ρx(C)/m(C)	ρx(Fe)/m(Fe)
#1$	#"!2 $	!"!+1 $
#0$	#"!($	!"!+/ $
#/ $	#"!/ $	!"!+/ $
#($	#"!- $	!"!+# $
#- $	#"!/ $	!"!+# $
##$	#"!($	!"!+# $
#! $	#"!/ $	!"!2; $
2$	#"!- $	!"!+# $
+$	!";; $	!"!+# $
; $	#"!! $	!"!+# $
1$	#"!0 $	!"!2; $
0$	#"!! $	!"!+# $
/ $	#"!- $	!"!+- $
#$	#"!/ $	!"!+# $
- $	#"!/ $	!"!+# $
($	#"!/ $	!"!+# $

8. UV/VIS/NIR Transmission Measurements

Filters for X-ray detectors in space are necessary to attenuate out of band radiation mainly in the UV/VIS/NIR. Transmission measurements performed in this wavelength band are necessary to constraint the transmission modelling and also to provide useful information such as: material thicknesses, metal oxidation, contamination, and aging.

The optical spectroscopy characterization of several TO8 frame filter samples was performed in UV-VIS-IR bands using a Jasco V770 optical spectrophotometer in transmission geometry at room temperature in ambient pressure at the Department of Physic and Chemistry of the University of Palermo.

First, a suitable sample holder was custom designed and realized to ensure samples were mounted always in the same position. The measurement parameters were optimized repeating transmission measurements for each filter to reduce noise and increase the accuracy. The optimized measurement parameters used to record the spectra are:

$

- Wavelength range: 190 – 3200 nm;
- Wavelength scan rate: 400 nm/min;
- UV-VIS bandwidth: 1 nm;
- NIR bandwidth: 4 nm;
- Data pitch: 0.5 nm.

$
#./"0+/#.$1234.51 $

The following filters have been investigated with this technique:
$
- TO8 C2-1 (C2 series pristine sample);
- TO8 C3-9 (C3 series pristine sample);
- TO8 C2-5 (1 x QF irradiated C2 series);
- TO8 C3-13 (1 x QF irradiated C3 series)
- TO8 C2-2 (10 x QF irradiated C2 series);
- TO8 C3-10 (10 x QF irradiated C3 series).

$
In order to calculate absolute filter transmission values and verify the spectrophotometer light source emission intensity trend with time, several blank spectra (with a dummy filter inserted) were acquired at the beginning of each sample measurement session. Each filter was measured more times (at least three times) to reduce the noise by averaging obtained spectra.

It was observed that noise became too high at wavelength greater than 3000 nm, as a consequence only the 190 – 2800 nm portion of the acquired spectra are taken into account to evaluate filter performances. The main results are summarized in table 26.

Table 26: Main difference between pristine and irradiated samples of the C2 and the C3 series.

Series	Sample	UV transmission peak position (nm)	UV transmission peak amplitude (%)
,- $	,- .#$OD>@F$@L	(!/ $	-+"(1- $
$	,- .0$O#$&"$$Q	(!/ $	#-"#2($
$	,- .-$O#!$&"$"$Q	-;; $	#("//1 $
,($	,(.;$OD>@F$@L	-//"0 $	-1"1(! $
$	,(.#($O#$&"$'$Q	-// $	-1"(/# $
$	,(.#!$O#!$&"$""$Q	-(; $	-1"/#+ $

From the UV-VIS-NIR point of view, the pristine and the 1 x QF irradiated samples are quite similar to each other while the pristine and the 10 x QF irradiated samples are different especially in the UV region. Figures 39 and 40 show the measured transmission curves in UV/VIS and NIR, respectively, for the C2 series.

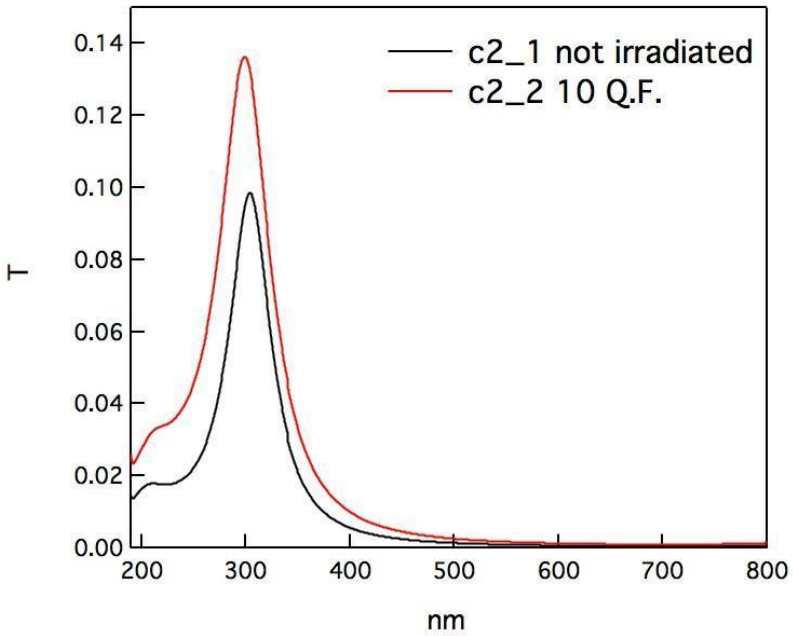

Fig. 39 – UV spectra of C2-1 (pristine) and C2-2 (10 x QF) filters. The UV peak shifts from 304 nm to 299 nm going from pristine to irradiated sample.

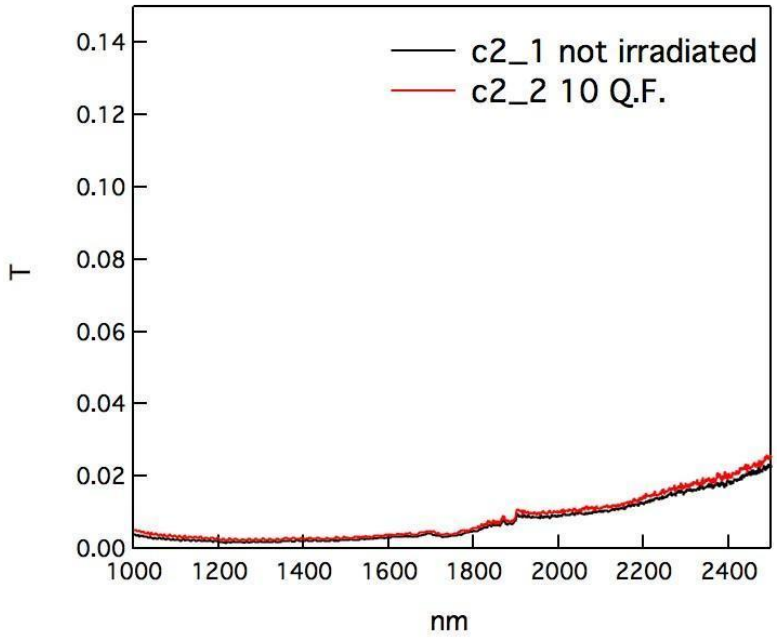

Fig. 40 – NIR spectra for both C2-1 (pristine) and C2-2 (10 x QF) filters.

The peak close to 300 nm is reasonably ascribable to the plasmon of aluminum (TBC). Such a signal blue-shifts if the samples are irradiated with 10 MeV protons with a fluence of 10 x QF, furthermore the thicker samples (c2 series) becomes more transparent.

#./)+%/#.$1234.51 $

Three kinds of CNT samples were characterized as a function of the density of the CNT's pellicle, named low-, medium-, and high-density.

Preliminary optical spectroscopy characterization of small low density CNT samples mounted on TF111 frames have also been performed in UV-VIS-IR bands using a Jasco V770 optical spectrophotometer in transmission geometry at room temperature in ambient pressure at the Department of Physic and Chemistry of the University of Palermo.

Figure 41 and 42 show a comparison between the measured transmission of CNT samples coated with aluminum split in equal amounts on both sides compared with the measured transmission for a thin polyimide filter with nearly the same amount of aluminum deposited on a single side or split in two sides.

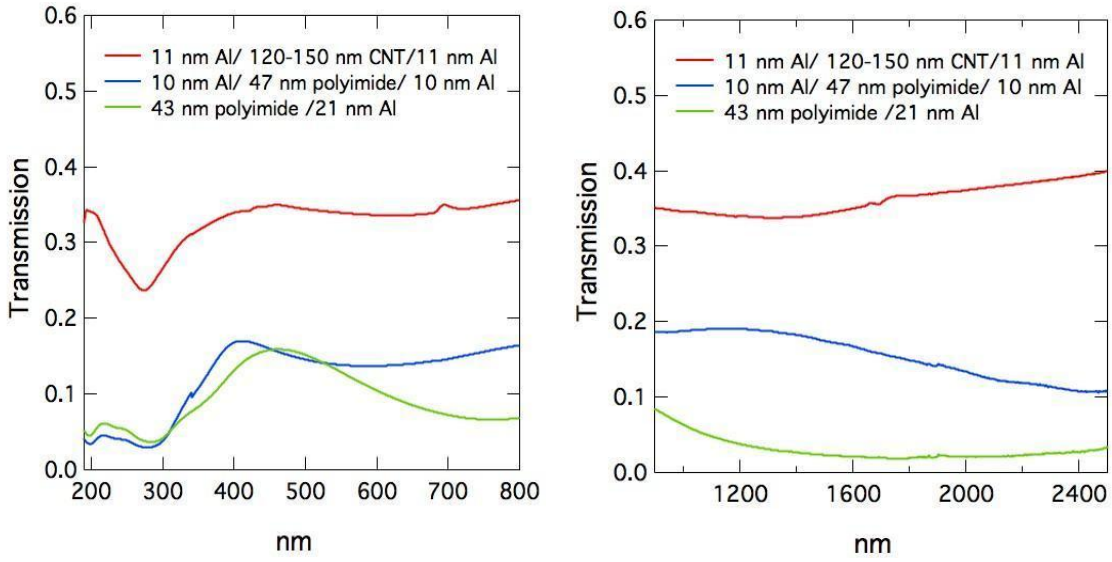

Fig. 41 – UV/VIS (left panel) and NIR (right panel) measured transmission for a low-density CNT filter samples with nearly 22 nm of aluminum coating split on the two sides, compared with the measured transmission for a polyimide filter coated with nearly the same amount of aluminum deposited on a single side or split in two sides.

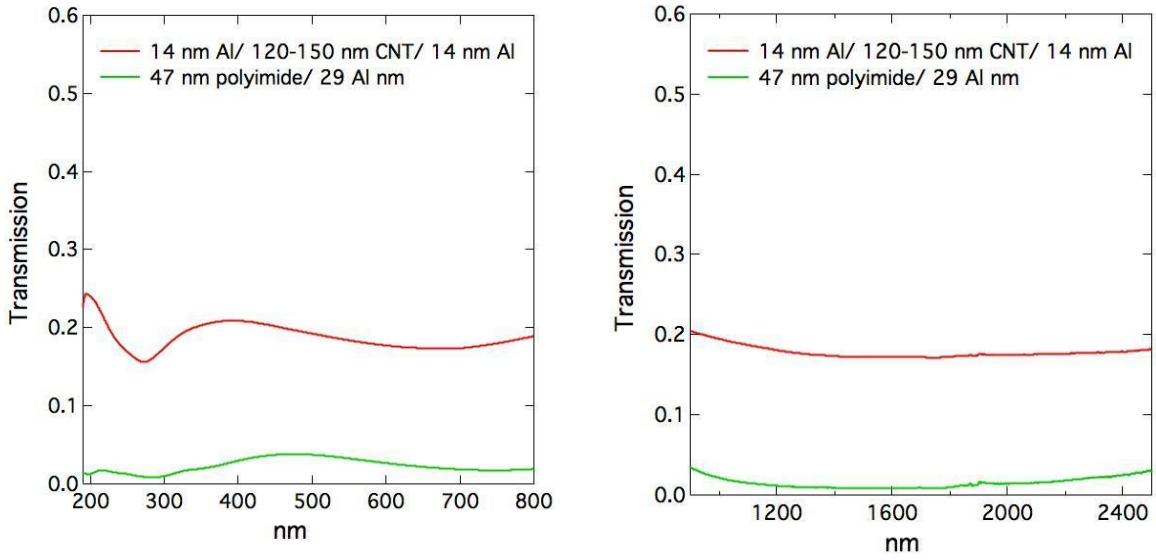

Fig. 42 - UV/VIS (left panel) and NIR (right panel) measured transmission for a low-density CNT filter samples with nearly 30 nm of aluminum coating split on the two sides, compared with the measured transmission for a polyimide filter coated with nearly the same amount of aluminum deposited on a single side.

The measured UV/VIS/NIR transmission for low-density CNT samples is significantly higher than what is measured on polyimide filters coated with aluminum. To reduce the transparency in the UV/VIS/NIR spectral range, medium- and high-density samples coated with aluminum on a single side were lately fabricated and studied.

In September 2020, an UV/VIS/NIR spectroscopic campaign was carried out to characterize a set of medium- and high-density bare and Al-coated CNT pellicles. All these samples present a transmittance of 90% at 550 nm meaning that the product **ρ***x is the same (**ρ** is the density, and x is the optical path length). We can thus hypothesize that the high-density samples are thinner than the medium-density samples, however, having the same **ρ***x they should be similar from a spectroscopic point of view. The measured samples are listed below:

$

- LAOF-CNT2-C2B2-F01 medium density 80 s
- LAOF-CNT2-C2B2-F02 medium density 56 s
- LAOF-CNT2-C2B2-F03 medium density 0 s
- LAOF-CNT2-C2B2-F04 high density 80 s
- LAOF-CNT2-C2B2-F05 high density 56 s
- LAOF-CNT2-C2B2-F06 high density 0 s

$

According to the supplier, the rate of aluminum deposition is 0.5 nm/s, then we characterized samples with no Al, with 28 nm of Al, and with 40 nm of Al. In figs 43 and 44, the acquired spectra are reported.

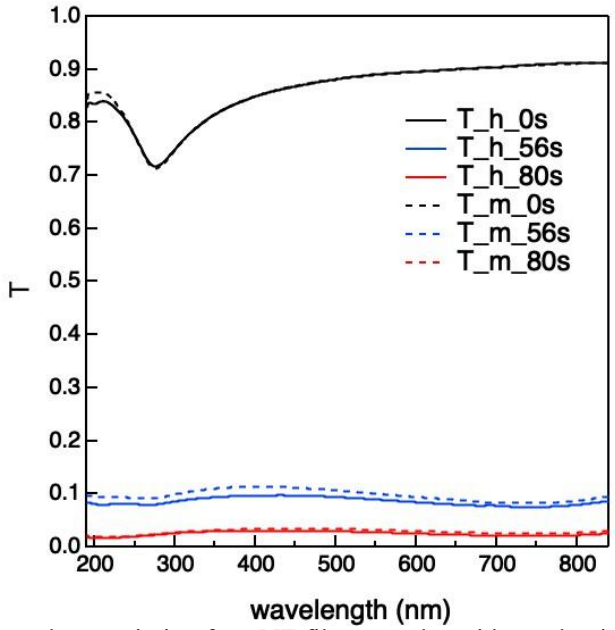

Fig.43 – UV/VIS measured transmission for CNT filter samples with no aluminum (black lines), with 28 nm (blue lines) and 40 nm (red lines) of aluminum coating on one sides of a high (solid lines) and medium density (dashed lines) pellicles.

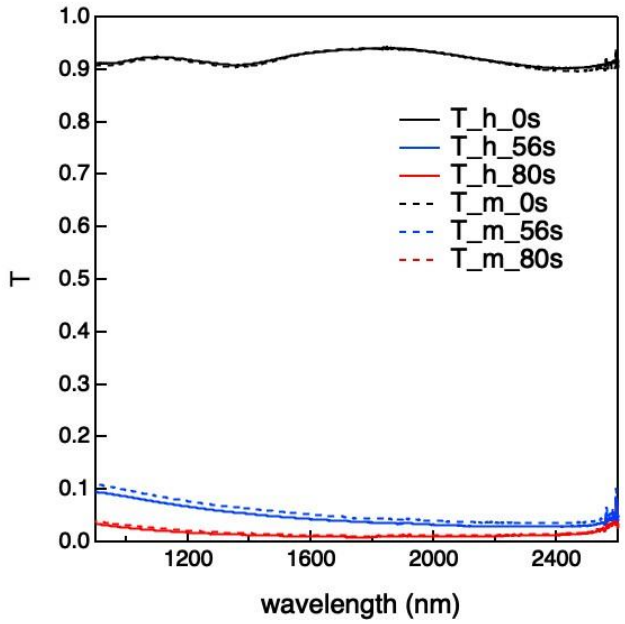

Fig.44 – NIR measured transmission for CNT filter samples with no aluminum (black lines), with 28 nm (blue lines) and 40 nm (red lines) of aluminum coating on one sides of a high (solid lines) and medium density (dashed lines) pellicles.

As expected, the transmittance of the LAOF-CNT2-C2B2-F03 and LAOF-CNT2-C2B2-F06 is quite similar in all the spectral ranges. The bare CNT pellicles are highly transparent in this spectral range showing an absorption peak in the UV close to 270 nm. On the other hand, the presence of a single coating of aluminum is quite efficient to reject the UV/VIS/NIR radiation.

Summing up, these preliminary measurements show that Al-coated high density and medium density CNT pellicles can reject out-of-band photons more efficiently than the low density samples, in addition single side aluminum coating is more efficient that double side coating. The UV/VIS/NIR rejection is though not as good as it is the case for continuous films like polyimide or Si_3N_4 coated with aluminum. Further investigation on this subject will part of the LAOF-CCN specifically dedicated to CNT based filters.

9. Radio Frequency Attenuation

The TES micro-calorimeter detectors and SQUID based read-out electronics used in the ATHENA X-IFU are very sensitive to electromagnetic interferences. For this reason, the thermal filters that need to attenuate the radiative heat load onto the X-IFU have also to provide an attenuation (approx 70 dB) of RF EMI in the 30 MHz-18 GHz range coming from the uplink/downlink X-band telemetry and satellite operation signals. Measurements of RF attenuation of filters coated with a thin metal layer, both self-standing and mesh supported, are needed to confirm the model predictions.

As part of the activities of the contract we have, in particular, investigated the capability of a thin layer of aluminum to attenuate RF when the filter is mounted on a Faraday shield. The RF attenuation measurement set-up used in this activity has been described in TN9.

The RF attenuation measurements reported in this technical note have been performed on a metal mesh and a set of filters with different thickness of aluminum. The mesh with honeycomb pattern is made of copper on FR4 support (fiberglass reinforced resin), a sample is reported in figure 45. The mesh has an aperture diameter of 56 mm, pitch = 4 mm, thickness = 35 μm, and bars width = 200 μm. The mesh is screw-mounted on a 100 mm diameter aluminum ring adapter that can be placed in the measurement setup.

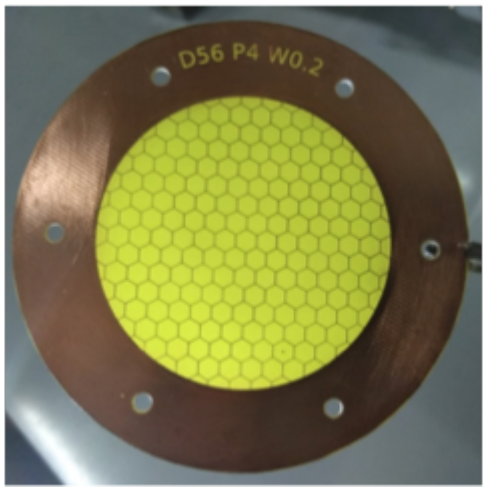

Fig. 45 - Hexagonal copper mesh on FR4 substrate. Mesh dimensions: diameter 56 mm, pitch 4 mm, thickness 35 μm, bars width 200 μm.

The aluminum filters are made of 90 μm thick Adwill D-675 insulating tape, coated with different thickness of aluminum. They are mounted on 100 mm diameter copper ring frames. The nominal

thickness of the aluminum coating for the different filters is 10 nm, 20 nm, 30 nm and 40 nm single sided and one sample 10 nm + 10 nm split on both sides of the plastic foil. A non-coated filter was also used as reference (figure 46).

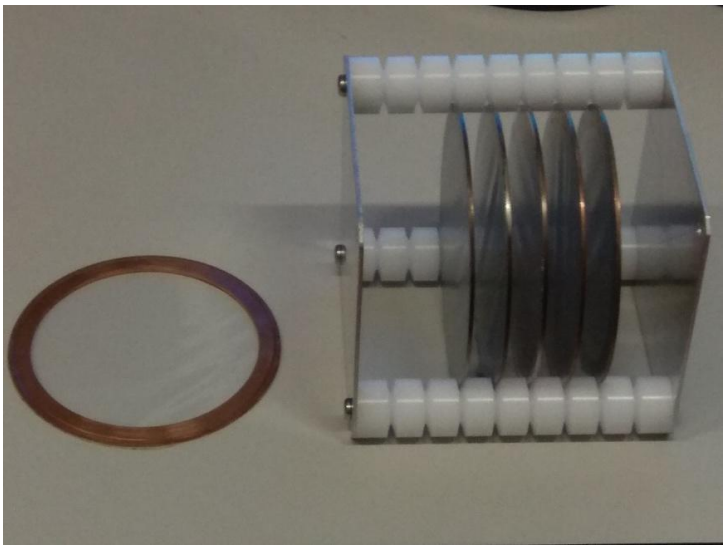

Fig. 46 - Aluminum thin film filters with different Al coating thickness on insulating tape.

The combination of every Al filter and the mesh was also tested. The mechanical and electrical coupling between mesh and each Al filter was obtained by mounting them on the two sides of a 3 mm thick aluminum disc, with a 56 mm diameter hole. Between mesh and Al filter there is, therefore, a 3 mm gap.

The measurements were divided in two sets: the first one with only aluminum coated filters and the second one with the mesh coupled with the aluminum filters. For each set of measurements, a reference without filter and one with a 3 mm thick aluminum disc were measured.

The antennas, mounted in the "L" shape configuration to excite both TE and TM modes, were connected to the two ports of a Keysight N5232A PNA-L Microwave Vector Network Analyzer (VNA) operating in the frequency range 300 kHz-20 GHz. The VNA was calibrated at the antenna connections, using the "SOLT" (Short, Open, Load, Thru) procedure. The adopted VNA settings were:

- Frequency span: 0.5-20 GHz;
- Sweep mode;
- Step: 25 MHz (781 points);
- IF BW: 100 kHz;
- Averaging: 100;
- No smoothing;
- Power: 0 dBm;
- Attenuator: 0 dB.

The described setup can be used with both frequency stirring or mechanical mode stirring, however, sliding the cavity walls can cause stress on both connectors and cables connecting the VNA to the antennas, impairing the readings accuracy.

To compare the two stirring methods, a preliminary test at low frequency (up to 3 GHz), with less critical cables and connectors, was performed using an Agilent N9320B Spectrum Analyzer.

The mechanical mode stirring was obtained by slowly sliding the walls while continuously sweeping the frequency. The instrument was set to perform a max hold measurement, meaning that the maximum transmission value for each frequency over all sweeps was saved (max hold in figure 47).

A frequency mode stirring was also done by sweeping over frequencies without moving the walls (raw data in figure 47) and evaluating the signal envelope. We evaluated the envelope as the maxima in 400 MHz bands (16 measured points). This BW is large enough so that in the lowest band above cut-off (1.75-2.15 GHz) 6 modes are already supported, and more at higher frequencies. Both stirring methods provided very similar results (figure 47), therefore we performed the measurements using only frequency stirring.

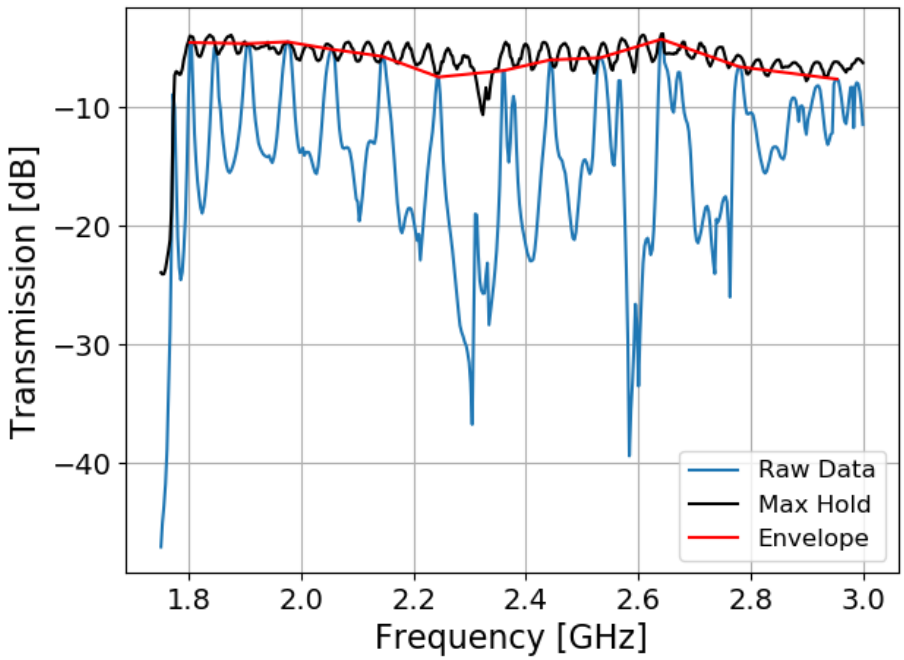

Fig. 47 - Comparison between SE evaluated by mechanical (max hold) and frequency (envelope) mode stirring, along with single frequency sweep raw data.

In order to verify the quality of the Al coatings and to extract parameters useful for future simulations, preliminary measurements of the surface resistances were performed. The measurements were done in different zones of the coated surface, using a gold plated 4-point probe and a 4-wire ohmmeter. The surface resistance (RS) was evaluated averaging the different measurements and using the expression:

$$R_s = R\frac{\pi}{\ln 2} = \frac{\rho}{T}$$

where R is the resistance measured by the ohm-meter, ρ is the resistivity and T the thickness of the conductive coating. The following values were found (table 27):

Table 27: Measured values of surface resistance, Rs, at different thicknesses,Tn, of the aluminum coating.

Tn (nm)	Rs (Ωsq)
#! $	#("! $
-! $	("21 $
(! $	-"!/ $
/! $	#"/# $

Aluminum coatings are subject to oxidation when exposed to air. The aluminum oxide has very high resistivity, therefore the conductive thickness of the coating is thinner than the nominal thickness. The resistivity of the conductive part of the coating is usually higher than the resistivity of pure aluminum because the coating is not as compact as the bulk material.

The surface conductance is:

$$G_S = \frac{1}{R_S} = \frac{T}{\rho} = \frac{T_n - T_0}{\rho}$$

Where T_n is the nominal thickness and T_0 is the thickness of the aluminum oxide. From the model fitting on the measured values the following results were obtained (figure 48):

$

- $GS = 0.021 T_n – 0.145 [1/Ωsq]
- $ρ = 1 / 0.021 = 47.6 Ω nm (pure bulk aluminum: ρ ~28 Ω nm)
- $$T_0$ = 0.145 / 0.021 = 6.9 nm

$

The calculated oxide thickness is in good agreement with oxide thickness measurements performed with different methods on aluminum filter samples.